Rapid fabrication of 3D terahertz split ring resonator arrays by novel single-shot direct write focused proximity field nanopatterning

Jonathan P. Singer,[1,2,*] Jae-Hwang Lee,[1,2,3] Steven E. Kooi,[2] and Edwin L. Thomas[1,2,3]

[1]*Department of Materials Science and Engineering, Massachusetts Institute of Technology, 77 Massachusetts Avenue, Cambridge, Massachusetts 02139, USA*

[2]*Institute for Soldier Nanotechnologies, Massachusetts Institute of Technology, 500 Technology Square, Cambridge, Massachusetts 02139, USA*

[3]*Currently with the Department of Mechanical Engineering and Materials Science, Rice University, Houston, Texas 77005, USA*

[*]*jpsinger@mit.edu*

Abstract: For the next generation of phoXonic, plasmonic, opto-mechanical and microfluidic devices, the capability to create 3D microstructures is highly desirable. Fabrication of such structures by conventional top-down techniques generally requires multiple time-consuming steps and is limited in the ability to define features spanning multiple layers at prescribed angles. 3D direct write lithography (3DDW) has the capability to draw nearly arbitrary structures, but is an inherently slow serial writing process. Here we present a method, denoted focused proximity field nanopatterning (FPnP), that combines 3DDW with single or multiphoton interference lithography (IL). By exposing a thick photoresist layer having a phase mask pattern imprinted on its surface with a tightly focused laser beam, we produce locally unique complex structures. The morphology can be varied based on beam and mask parameters. Patterns may be written rapidly in a single shot mode with arbitrary positions defined by the direct write, thus exploiting the control of 3DDW with the enhanced speed of phase mask IL. Here we show the ability for this technique to rapidly produce arrays of "stand-up" far IR resonators.

OCIS codes: (140.3390) Laser materials processing; (220.4000) Microstructure fabrication; (160.3918) Metamaterials.

References and links

1. S. Maruo and K. Ikuta, "Three-dimensional microfabrication by use of single-photon-absorbed polymerization," Appl. Phys. Lett. **76**(19), 2656–2658 (2000).
2. G. Witzgall, R. Vrijen, E. Yablonovitch, V. Doan, and B. J. Schwartz, "Single-shot two-photon exposure of commercial photoresist for the production of three-dimensional structures," Opt. Lett. **23**(22), 1745–1747 (1998).
3. M. Farsari, G. Filippidis, and C. Fotakis, "Fabrication of three-dimensional structures by three-photon polymerization," Opt. Lett. **30**(23), 3180–3182 (2005).
4. M. Deubel, G. von Freymann, M. Wegener, S. Pereira, K. Busch, and C. M. Soukoulis, "Direct laser writing of three-dimensional photonic-crystal templates for telecommunications," Nat. Mater. **3**(7), 444–447 (2004).
5. L. Li, R. R. Gattass, E. Gershgoren, H. Hwang, and J. T. Fourkas, "Achieving λ/20 resolution by one-color initiation and deactivation of polymerization," Science **324**(5929), 910–913 (2009).
6. M. Malinauskas, A. Zukauskas, G. Bickauskaite, R. Gadonas, and S. Juodkazis, "Mechanisms of three-dimensional structuring of photo-polymers by tightly focussed femtosecond laser pulses," Opt. Express **18**(10), 10209–10221 (2010).
7. K. K. Seet, S. Juodkazis, V. Jarutis, and H. Misawa, "Feature-size reduction of photopolymerized structures by femtosecond optical curing of SU-8," Appl. Phys. Lett. **89**(2), 024106 (2006).
8. M. Thiel, J. Fischer, G. von Freymann, and M. Wegener, "Direct laser writing of three-dimensional submicron structures using a continuous-wave laser at 532 nm," Appl. Phys. Lett. **97**(22), 221102 (2010).

#164825 - $15.00 USD Received 16 Mar 2012; revised 19 Apr 2012; accepted 26 Apr 2012; published 30 Apr 2012

9. J. Fischer, G. von Freymann, and M. Wegener, "The materials challenge in diffraction-unlimited direct-laser-writing optical lithography," Adv. Mater. (Deerfield Beach Fla.) **22**(32), 3578–3582 (2010).
10. J. Scrimgeour, D. N. Sharp, C. F. Blanford, O. M. Roche, R. G. Denning, and A. J. Turberfield, "Three-dimensional optical lithography for photonic microstructures," Adv. Mater. (Deerfield Beach Fla.) **18**(12), 1557–1560 (2006).
11. S. Jeon, D. J. Shir, Y. S. Nam, R. Nidetz, M. Highland, D. G. Cahill, J. A. Rogers, M. F. Su, I. F. El-Kady, C. G. Christodoulou, and G. R. Bogart, "Molded transparent photopolymers and phase shift optics for fabricating three dimensional nanostructures," Opt. Express **15**(10), 6358–6366 (2007).
12. J. P. Singer, S. E. Kooi, and E. L. Thomas, "Focused laser spike (FLaSk) annealing of photoactivated chemically amplified resists for rapid hierarchical patterning," Nanoscale **3**(7), 2730–2738 (2011).
13. M. Li, K. Douki, K. Goto, X. Li, C. Coenjarts, D. M. Smilgies, and C. K. Ober, "Spatially controlled fabrication of nanoporous block copolymers," Chem. Mater. **16**(20), 3800–3808 (2004).
14. H.-W. Li and W. T. S. Huck, "Ordered block-copolymer assembly using nanoimprint lithography," Nano Lett. **4**(9), 1633–1636 (2004).
15. S. A. Pruzinsky and P. V. Braun, "Fabrication and characterization of two-photon polymerized features in colloidal crystals," Adv. Funct. Mater. **15**(12), 1995–2004 (2005).
16. S. A. Rinne, F. Garcia-Santamaria, and P. V. Braun, "Embedded cavities and waveguides in three-dimensional silicon photonic crystals," Nat. Photonics **2**(1), 52–56 (2008).
17. S. Jeon, J.-U. Park, R. Cirelli, S. Yang, C. E. Heitzman, P. V. Braun, P. J. A. Kenis, and J. A. Rogers, "Fabricating complex three-dimensional nanostructures with high-resolution conformable phase masks," Proc. Natl. Acad. Sci. U.S.A. **101**(34), 12428–12433 (2004).
18. C. H. Chang, L. Tian, W. R. Hesse, H. Gao, H. J. Choi, J. G. Kim, M. Siddiqui, and G. Barbastathis, "From two-dimensional colloidal self-assembly to three-dimensional nanolithography," Nano Lett. **11**(6), 2533–2537 (2011).
19. M. C. George, E. C. Nelson, J. A. Rogers, and P. V. Braun, "Direct fabrication of 3D periodic inorganic microstructures using conformal phase masks," Angew. Chem. Int. Ed. Engl. **48**(1), 144–148 (2009).
20. G. Bautista, M. J. Romero, G. Tapang, and V. R. Daria, "Parallel two-photon photopolymerization of microgear patterns," Opt. Commun. **282**(18), 3746–3750 (2009).
21. K. B. Fan, A. C. Strikwerda, H. Tao, R. D. Averitt, and X. Zhang, "3D stand-up metamaterials with a purely magnetic resonance at terahertz frequencies," in *Mems 2010: 23rd Ieee International Conference on Micro Electro Mechanical Systems, Technical Digest*, (2010) pp. 843–846.
22. D. B. Burckel, J. R. Wendt, G. A. Ten Eyck, J. C. Ginn, A. R. Ellis, I. Brener, and M. B. Sinclair, "Micrometer-scale cubic unit cell 3D metamaterial layers," Adv. Mater. (Deerfield Beach Fla.) **22**(44), 5053–5057 (2010).
23. J. H. Cho, M. D. Keung, N. Verellen, L. Lagae, V. V. Moshchalkov, P. Van Dorpe, and D. H. Gracias, "Nanoscale origami for 3D optics," Small **7**(14), 1943–1948 (2011).
24. S. Zhang, W. Fan, B. K. Minhas, A. Frauenglass, K. J. Malloy, and S. R. J. Brueck, "Midinfrared resonant magnetic nanostructures exhibiting a negative permeability," Phys. Rev. Lett. **94**(3), 037402 (2005).
25. J.-H. Lee, C.-H. Kim, Y.-S. Kim, K.-M. Ho, K. Constant, and C. H. Oh, "Three-dimensional metallic photonic crystals fabricated by soft lithography for midinfrared applications," Appl. Phys. Lett. **88**(18), 181112 (2006).
26. F. Formanek, N. Takeyasu, T. Tanaka, K. Chiyoda, A. Ishikawa, and S. Kawata, "Three-dimensional fabrication of metallic nanostructures over large areas by two-photon polymerization," Opt. Express **14**(2), 800–809 (2006).
27. J. K. Gansel, M. Thiel, M. S. Rill, M. Decker, K. Bade, V. Saile, G. von Freymann, S. Linden, and M. Wegener, "Gold helix photonic metamaterial as broadband circular polarizer," Science **325**(5947), 1513–1515 (2009).
28. C. M. Soukoulis, T. Koschny, J. Zhou, M. Kafesaki, and E. N. Economou, "Magnetic response of split ring resonators at terahertz frequencies," Phys. Status Solidi, B Basic Res. **244**(4), 1181–1187 (2007).

1. Introduction

In order to advance lithographic capabilities for future applications, innovative strategies must be available in a scalable and cost-effective set of techniques. This is especially the case when approaching the fabrication of complex 3D architectures not amenable to conventional layer-by-layer processing, such as those with angled features extending through multiple layers. The ability to pattern 3D structures of controllable position, size, and symmetry across multiple length scales will enable a new generation of optical, acoustic, mechanical, plasmonic, electronic, and other devices. One promising technique for nearly arbitrary fabrication of 3D structures is 3D direct write (3DDW). 3DDW utilizes focused light via single photon [1], multiphoton lithography [2–5], or other non-linear effects [6–8] within a photoresist or other photosensitized medium to achieve subwavelength resolution ($\lambda/4$ down to $\lambda/20$ with new stimulated emission depletion microscopy inspired techniques [5,9]), but at the cost of slow, serial patterning.

Recently, local direct write, microimprint, or UV photomasking performed on materials with latently defined patterns have been utilized to rapidly pattern 3D hierarchically

#164825 - $15.00 USD Received 16 Mar 2012; revised 19 Apr 2012; accepted 26 Apr 2012; published 30 Apr 2012

structured samples. Some notable examples include the introduction of purposeful defects or creation of local hierarchical structures in 3D media patterned either by interference lithography (IL) [10–12], or colloidal/block copolymer self-assembly [13–16]. All of these techniques are capable of fabricating structures with periodic or quasiperiodic substructures that could only be patterned by 3DDW, but at a fraction of the time. In these techniques, however, the structures formed during a single fabrication step are limited to the substructure defined by the latent, large area (IL/self-assembly) pattern, possibly with limited variation in the fill fraction [12], and further, require the execution of a 3D patterning process in order to enable the local patterning, which adds complexity to the overall procedure. Our approach combining 3DDW and soft-lithography proximity field nanopatterning [11, 17, 18] allows for the fabrication of multiple varieties of local 3D structures in single shot exposures controlled by the beam parameters (wavelength, numerical aperture (NA), point spread function (PSF), and focus) of the direct write process superimposed with the latent pattern created by the interference of the diffraction orders of the surface mask.

Soft-lithography proximity field nanopatterning (PnP) has been used as a technique to increase the dielectric contrast and pattern control of conventional phase mask interference lithography. Surface masks, made by either imprint [11, 19] or nanoparticle self-assembly [18], have been utilized to make macroscale and, in combination with local heating [12], microscale periodic and quasiperiodic structures with micron to submicron feature size. This was performed through the application of nearly plane-wave incident light illumination through the surface mask with either single or multiphoton photoactivation. This technique departs from conventional phase mask lithography by utilizing a soft-lithographic process to generate a proximal 2D surface relief pattern, the entirety of which is the active optical element, as opposed to having an optically interacting stamp volume. The innovation of the presented technique, referred to here as focused proximity field nanopatterning (FPnP), is replacing the global optical exposure with a local focused source. In this way, localized patterns based on a combination of the beam parameters and the diffraction orders of the surface mask can be defined in a single shot.

A schematic of the steps of the FPnP process is shown in Fig. 1. Each given mask and set of beam parameters allows for a family of patterns, each with a similar angular profile but differing overall size, to be generated depending on the focal position relative to the mask. FPnP is easily combinable with PSF manipulation, such as that recently demonstrated for the single shot fabrication of gear-like structures [20]. Simple modifications to the technique can

#164825 - $15.00 USD Received 16 Mar 2012; revised 19 Apr 2012; accepted 26 Apr 2012; published 30 Apr 2012

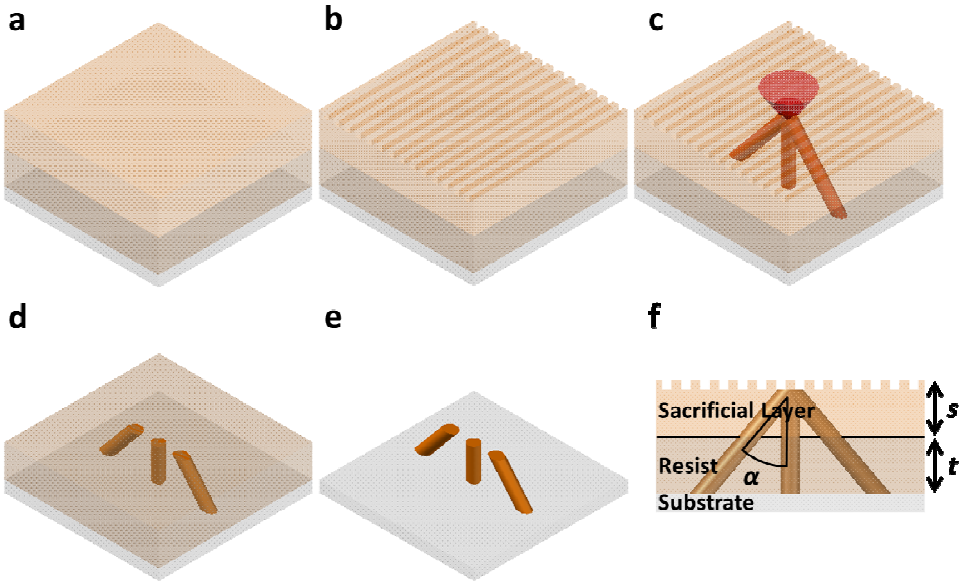

Fig. 1. Scheme for FPnP. (a) Photoresist and optional sacrificial layer are spin coated sequentially onto the substrate. (b) At elevated temperature (>60 °C) the surface mask is imprinted into the top surface. (c) FPnP patterning is performed by multiple single shot exposures. (d) Sacrificial layer is removed, at this point another cycle of patterning and/or 3DDW can be performed, after final patterning post exposure bake is executed. (e) Sample is developed leaving the final structure. (f) Cross-section of patterning with key parameters, resist and sacrificial layer thickness (t and s), and branch angle (α) indicated.

allow for multiple patterning steps. For example, *in situ* removal of the surface mask can allow for consecutive, registered 3DDW to enable incorporation of features disparate from those defined by the mask. Additionally, use of a sacrificial layer (SL) can allow for cross-sectional control of the patterns formed.

Structures made by this process all share some key similarities in their morphology due to their origin and thus represent a reduction in the arbitrary freedom of 3DDW; however, these patterns may be produced orders of magnitude faster depending on beam parameters and the fabrication system. Thus, one needs to understand the nature and range of types of motifs that are accessible by FPnP and note promising structural and materials composite applications. "Stand-up" plasmonic microresonators, which generally requires detailed, many-step fabrication processes [21–24], are one such application area.

2. Experimental

The photoresist utilized in this study was commercially available negative tone SU-8 2005 (Microchem). The SL was made utilizing 20 wt% low molecular weight polystyrene (2 k, Fluka) dissolved in cyclohexane (Sigma-Aldrich). All materials were used as received, with the exception of SU-8, to which, for some experiments, 0.5 wt% of 2- isopropyl thioxanthone was added as a multiphoton sensitizer. This allowed for shorter exposures, but also had some effect on the overall shape of the structures.

For FPnP, SU-8 was spun onto a substrate consisting of a previously crosslinked adhesion layer (<1 μm) of SU-8 on a glass coverslip with a 500 rpm spreading spin (10 s) followed by a 1500-3000 rpm spin (30 s). The spin speed determined the thickness of the FPnP sample. Soft bake was then performed at 95 °C for 5-15 min. After soft bake, polystyrene SL was then spun on with a similar 1500-3000 rpm spin. Next, a PDMS phase mask is brought into contact at room temperature and then imprinted with light pressure manually at 95 °C for ~10 s to form a replica of the phase mask pattern. FPnP patterning and 3DDW were both performed

#164825 - $15.00 USD Received 16 Mar 2012; revised 19 Apr 2012; accepted 26 Apr 2012; published 30 Apr 2012

utilizing 780 nm light from a Coherent RegA Ti:Sapphire oscillator laser system utilizing an 80 MHz rep rate with 160 fs pulses. Continuous wave 532 nm exposure was performed with a Coherent Verdi-V5 laser. Power was controlled by a neutral density filter and measured with a power meter (Newport 818-UV) using a removable mirror placed before the lens. Exposures are shown for near IR with focus 2-4 μm below the grating were performed between 25 and 45 mW of power depending on the thickness of the sacrificial layer for 400 or 800 ms while the sample with focus 8 μm above the grating was performed at 75 mW for 8.1 s. Structures fabricated with green light were made with 800 ms exposures at 85 mW. The lens used was a 40X objective of numerical aperture (NA) of 0.7. The last optic before the objective was a near IR and green dual-band dielectric mirror, allowing for simultaneous imaging in transmission with red (600-700 nm) light via a camera mounted above the stage. Motion of the sample for direct write was controlled by a Physik Instruments PIMars piezostage with 300 μm of travel on all three axes mounted on a course micrometer stage for larger motion. Patterning was controlled by a LabView program that controlled both the piezostage and an electronic shutter. Samples shown were generated with 400 ms single shot exposures at various powers. After exposure, post exposure bake was performed with 1 min at 65 °C and 1 min at 95 °C. Sample development was done by immersion in propylene glycol methyl ether acetate (PGMEA) for 10-20 minutes, followed by immediate dipping in isopropyl alcohol (IPA) to rinse the PGMEA and development byproducts. IPA doubly serves to rinse to act as a lower surface tension solvent to limit the capillarity induced collapse of the written structures. For consecutive 3DDW, surface pattern was cleared by 10 s hotplate heating at 95 °C and then realigned by eye using the contrast of the previously written structures.

Scanning electron microscopy (SEM) was performed on a JEOL 6060 at an accelerating voltage of 5 keV. All images presented were taken at a 30° tilt.

To prepare samples for optical resonance measurement 45-60 nm of gold were deposited at 45° four times with 90° rotation between each deposition using a Desk II Sputterer (Denton Vacuum). Far-IR FTIR Measurements were performed on the U12A IR beamline at the National Synchrotron Light Source at Brookhaven National Laboratory. Samples were measured on a Continuμm IR microscope (Thermo Scientific) in reflection geometry using polarized light and a Si bolometer detector. The objective utilized for the measurements was a Schwarzschild-style NA = 0.58, 15X objective. Scans were taken with 4 cm^{-1} spectral resolution, and surrounding flat metalized area was utilized as reflection reference.

Finite element method (FEM) simulations were performed with COMSOL Multiphysics 4.1 Electromagnetic Waves Module. 2D simulations of FPnP intensity distributions were performed in a 20 μm square cell with scattering boundary conditions. 9.5 μm of air above 5 μm of resist placed on 5.5 μm of glass are used as the sample. Laser illumination is simulated using the analytical Gaussian equation with polarization of the electric field perpendicular to the cell. 3D resonator simulations are performed with a 15 μm cube cell with periodic boundary conditions in the *X* and *Y*. Substrate and structure are simulated as effective impedance boundary using the conductivity of gold ($4x10^7$ S m^{-1}). To attempt to match the Schwarzschild-style objective to reproduce the experimental results, tilted incidence was used at 35.5°, which is the edge of the light cone for the objective.

3. **Fabrication of structures by FPnP**

Any phase mask process is governed by the diffraction of the incident light by the periodicity of the mask into various beam orders. In the near-field, these beams interfere to produce the 3D pattern. The general 1D diffraction equation for light entering a resist from air is:

$$a\left(\sin\theta_i + n\sin\theta_d\right) = m\lambda \tag{1}$$

Where a is the periodicity of the mask, $\theta_{i/d}$ is the incident/diffracted angle of the light, n is the refractive index of the resist, m is the order of the diffraction and λ is the incident wavelength.

#164825 - $15.00 USD Received 16 Mar 2012; revised 19 Apr 2012; accepted 26 Apr 2012; published 30 Apr 2012

In typical phase mask IL, $\theta_i = 0$ leading to symmetric interference of the positive and negative orders dependent on the ratio of the mask spacing and the illumination wavelength. In FPnP, however, there are a range of angles in the convergent/divergent beam, and also a beam width at the grating on the order of the lattice parameter or less leading to a low resolvancy. The spot size incident on the grating of the Gaussian plane wave focused by the objective lens can be determined by the following:

$$w \approx \frac{\lambda}{\pi NA}\sqrt{1+\left(\frac{\pi NA^2}{\lambda}Z\right)^2} \tag{2}$$

where Z is the distance of the grating from the focal plane. The FPnP process possesses several degrees of freedom in both the positioning and the final morphology of the fabricated structures, all of which involve the manipulation of elements in either Eq. (1) or Eq. (2). Below we will concentrate on structures produced by FPnP on 1D grating masks for ease of simulations; however, the concepts discussed are equally applicable to 2D masks with the main important consideration being that the greater number of diffracted beams reduces the fraction of the intensity in each.

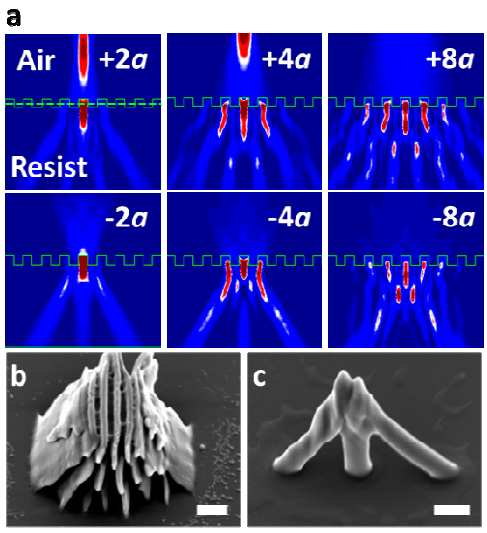

Fig. 2. (a) 2D finite elements simulation of two-photon intensity pattern from 0.78a wavelength light with varying focus through a a/2 square wave surface imprint. Top row from left to right is focused placed 4a, 8a, and 12a above the imprint midpoint (indicated by dashed line). Bottom row is 4a, 8a, and 12a below the midpoint. (b-c) tilted (30°) SEM images of two SU-8 structures fabricated at different focus heights with 780 nm light and a = 1 μm. (b) Focus 8 μm above, is representative of interference dominated structures, while (c) focus 2 μm below, is representative of diffraction dominated. (Scale bars 2 μm).

3.1. Control of structure by variation of focal position

As discussed, the primary difference between conventional PnP and FPnP is that the plane wave exposure source is replaced by a focused beam. Figure 2 depicts 2D FEM simulations of the two-photon intensity pattern from an 780 nm light source focused (NA 0.7) through a 1 μm periodic square surface grating imprinted 0.5 μm deep into a 5 μm thick photoresist (SU-8 2005, Microchem Inc.). It should be noted that that all of these parameters are scalable, and thus may be considered in units of the grating period assuming, as in these simulations, that the wavelength dependent optical properties of the resist such as a characteristic absorption curve are not considered. There are several clear varieties of local patterns in intensity contrast. When the focus is just above or below the grating (<2X the mask period, Fig. 2(a)

#164825 - $15.00 USD Received 16 Mar 2012; revised 19 Apr 2012; accepted 26 Apr 2012; published 30 Apr 2012

top-left), the simulated pattern contains features dominated by the diffraction orders of the beam. By a combination of the beam size and divergence from a plane wave, the resultant diffraction occurs at a range on angles, with a net "branch" of high intensity occurring where the scattered light of various portions of the beam is most in phase, thus generating the maximal contrast for transfer to the resist. For these reasons, this effective diffraction angle, ~26°, is not that predicted by Eq. (1) (29.8°). In contrast to the near focus, as the focal plane gets further away from surface grating, the illumination area grows in size and the local pattern begins to take on the features of conventional interference. However, the resulting patterns possess tilted features due to the wide range of incident angles included in the convergent/divergent focused beam. As described below, a surface imprint can be created by pressing an elastomeric stamp into resist materials heated above their flow temperature. Examples of both types of structure fabricated in SU-8 utilizing a polydimethylsiloxane (PDMS) mask with the same dimensions as the simulation are also shown in Fig. 2(b), 2(c). Despite the 2D nature of the simulations, the experimental structures demonstrate excellent agreement with the simulated intensity distributions in their central cross-section as the 1D surface grating does not greatly alter the parallel beam distribution.

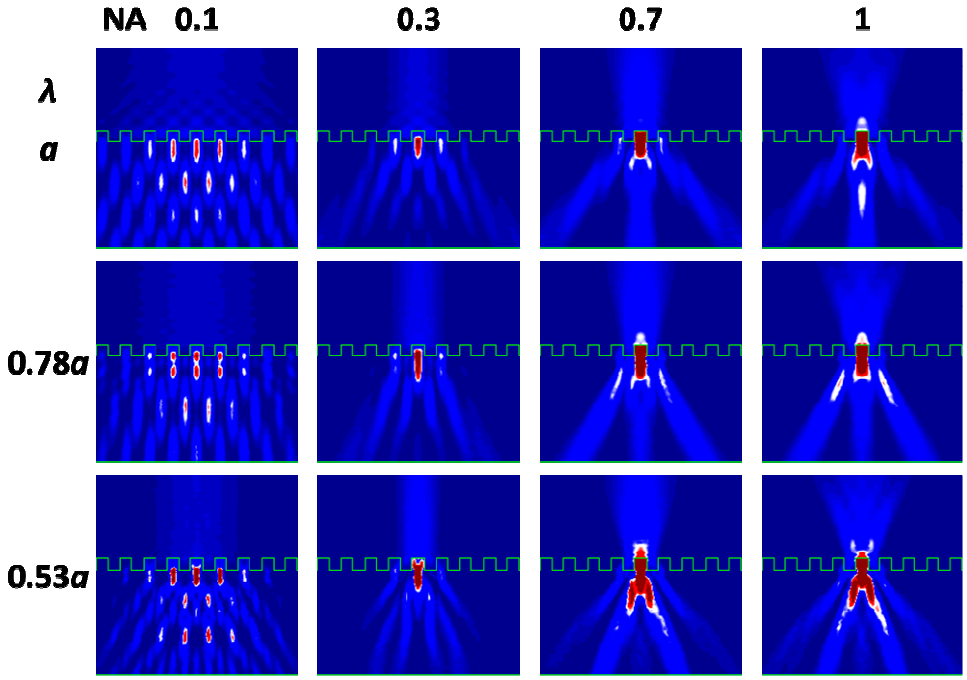

Fig. 3. FEM simulations of two-photon intensities for a variety of NA and λ values of a beam focused 2a below the surface of the structure described in Fig. 2. It can be seen that these two parameters can control the aspects (angles/number of beams, proportion of intensity in each beam) of the final intensity pattern.

3.2. Control of structure by beam parameters

While the focal position of the beam to a large extent determines the morphology that will be fabricated by the FPnP process, many characteristics of the structure are set by the beam wavelength and the objective's NA which controls/contributes to the range of incident angles of the illumination. Figure 3 shows a table of simulated intensity patterns at various normalized wavelengths and objective NAs for a given focus (2a below the grating center). Tuning of the laser wavelength changes the angle and number of diffracted orders as described in Eq. (1) and also changes the diffraction efficiency of the grating and thus the relative dose and feature size of the diffracted branches. For example, Fig. 4(a) shows the

#164825 - $15.00 USD Received 16 Mar 2012; revised 19 Apr 2012; accepted 26 Apr 2012; published 30 Apr 2012

transition from three to two branches by changing near IR to green 3DDW. In the case of the sub-imprint green light, the 0th order is relatively suppressed with respect to the 1st orders. This is an especially attractive method for tuning the structure as wavelength in most tunable laser systems can be set with a high degree of precision for single-degree alteration of the diffracted orders. The wavelength also affects the overall spot size, but to a lesser, linear extent. The effect of tuning NA can be more complex as it is coupled to both the spot size given by Eq. (2) and also determines the angular range of incident light, thus changing the effective branch angle; however altering the NA with the beam focus near the surface imprint mainly spreads the beam, resulting in patterns similar to that of the mask with plane wave illumination at low NA.

3.3. Sacrificial layer for cross-sectional control

In conventional IL, cross-sectional control as a concept is relatively unimportant – different sections of the intensity distribution are periodic along the incident axis, and therefore, any sizable portion of the resultant structure can be expected to exhibit similar physical properties. This is not the case for FPnP structures, which possess no axial periodicity. Due to this fact, distinct axial slices of FPnP structures will be different and this can lead to useful variations in their properties. In addition to cross-sectional control, another concept generally not critical for conventional IL is proximal positioning (including partial overlap) of multiple motifs.

A SL can be used to enable both of these additional levels of pattern control. A SL consists of a non-photoactive material deposited on top of the resist that is able to be imprinted without affecting the resist. In this way, the thickness of the SL can be used to control the top of the targeted structure, with the bottom portion controlled by the total bilayer thickness. SLs have been used in the past for isolation of 2D cross-sections from colloidal PnP utilizing resist separation by deposition of a thin layer of silica [18]. Rather than utilize an additional deposition technique and hydrofluoric acid etch as in the prior work, it would be preferable to identify a spin-coating-compatible SL material that was soluble in an orthogonal solvent to the resist. Additional important considerations for the SL include a similar refractive index and glass-transition temperature as the utilized resist so as to not cause distortion in the optical pattern or require incompatable processing respectively. A SL material which is suitable for our purposes is low molecular weight (<2.5 k) polystyrene, which is soluble in cyclohexane, a non-solvent for most resists. This allows the PS to be spun directly onto a resist layer and removed either with a predevelopment soak step in cylcohexane or in the same developer as the resist. More specifically, we utilized 2 k polystyrene possessing a glass transition temperature of ~60 °C allowing for imprinting at modest temperatures (<100 °C). The thickness of the SL was controlled by spin speed. Figure 4 shows structures patterned using polystyrene SLs demonstrating cross-sectional control.

3.4. Consecutive 3DDW

The enhanced patterning speed of FPnP comes at the cost of the arbitrary freedom of direct write; however, some targeted devices, while utilizing the structures of FPnP, may also require additional features not available from the FPnP motif. Since an FPnP system is already designed for direct write, consecutive 3DDW is an attractive option for defining these additional features. One way that this can be performed is by the thermal clearing of the surface imprint. By once again raising the resist/SL above the flow temperature, the surface

#164825 - $15.00 USD Received 16 Mar 2012; revised 19 Apr 2012; accepted 26 Apr 2012; published 30 Apr 2012

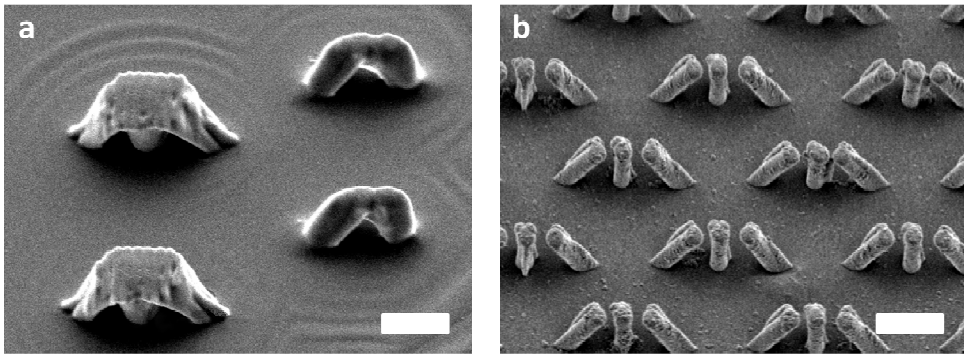

Fig. 4. Structures generated with two different thicknesses of sacrificial polystyrene layers. (a) Sample with reduced top grating, patterned with both NIR (left, 780 nm) and green (right, 532 nm) 3DDW. (b) An array of structures with removed top grating layer leading to gaps between the branches. (Scale bars 5 μm).

imprint quickly (~1-10s) smoothes by curvature driven flow. In the case of chemically amplified photoresists (CARs), such as the SU-8 employed in this study, this can be performed as a part of the post-exposure bake (PEB) either by removing, baking, and repositioning or ideally, performing the PEB with an integrated hot-stage. After erasing the original diffractive surface element, conventional, though relatively low NA, 3DDW may be performed (Fig. 5). The reason this is possible is that 3DDW in CARs often does not require its own PEB due to the high intensities involved [6, 7, 12]. Alternatively, in such applications where arbitrary high resolution (<500 nm) patterning is additionally necessary, 3DDW may be performed side by side by using top and bottom objectives and a transparent substrate to allow for oil immersion (NA>1).

4. FPnP microresonator structures

One area where FPnP structures are advantageous is the generation of "stand-up" microresonators. Resonators such as ring and split-ring produce their artificial-atom resonances by coupling the magnetic field of incident light into the induction of the ring. In split-ring resonators (SRRs), the presence of a capacitive gap acts to shift the resonance to longer wavelengths than the size of device and therefore allows for low-scattering coupling. One disadvantage to these SRRs is that for micro or nanoresonators fabricated by conventional lithographic techniques, it is simplest to pattern rings in the plane of the

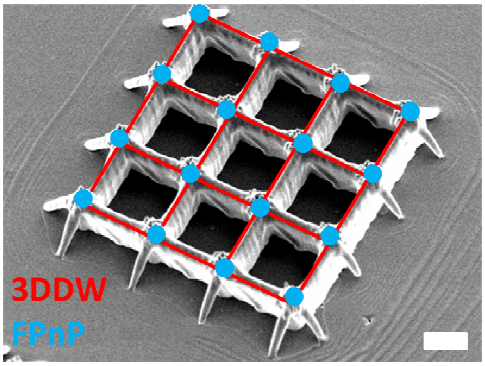

Fig. 5. Structures created by a sequence of FPnP, surface pattern clearing by heating, and subsequent registered MPL. Realignment for 3DDW patterning step after sample removal and heating was assisted by optical contrast which formed in the FPnP patterned areas after baking the resist due to shrinkage of the exposed resist. (Scale bar 5 μm).

#164825 - $15.00 USD Received 16 Mar 2012; revised 19 Apr 2012; accepted 26 Apr 2012; published 30 Apr 2012

substrate. As a result, the coupled light must also be in the same plane for the greatest effect on the magnetic properties (such as effective permeability). For most resonator applications, it would be preferable to couple into light incident perpendicular to the substrate by utilizing "stand-up" resonant structures. FPnP is an ideal technique for the fabrication of such structures via the design methods detailed above, combined with metallization by either by multi-angle coating [25], selective electroless-plating [26] of negative resist structures or backfill electrodeposition [27] of positive resist structures, which have all been previously utilized to generate plasmonic or photonic structures from 3D lithography.

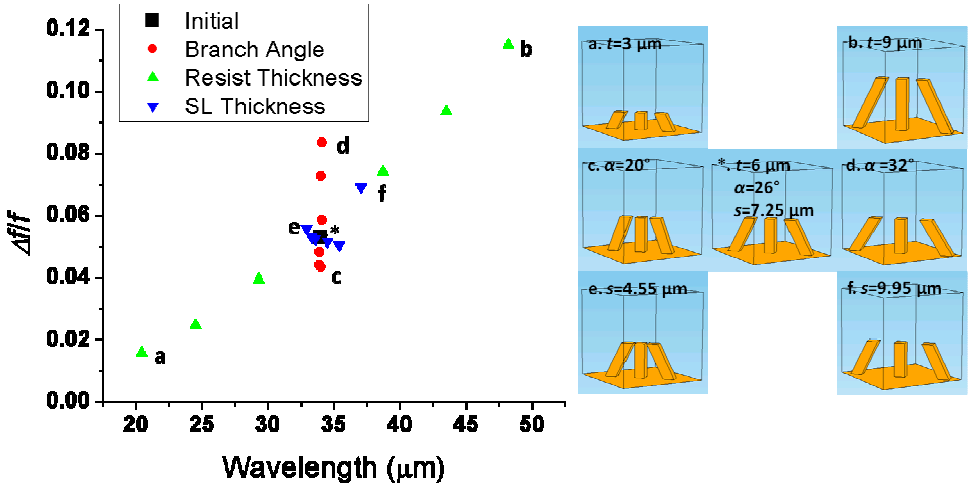

Fig. 6. FEM simulations of the resonant peak position (f) and normalized peak width ($\Delta f/f$) of arrays of "stand-up" resonators produced by FPnP with varying processing parameters. Initial orientation (*) was chosen to be a similar, simplified geometry to the devices shown in Fig. 4(b): 15 μm-period square arrays, 6 μm resist thickness (t), 780 nm exposure (leading to ~26° branch angle (α)), and 7.25 μm SL thickness (s). Starting from this configuration, t (a-b, 3-6 μm), α (c-d, 20-32°), and s (e-f, 4.55-9.95 μm) were varied to determine the effects of these parameters. Images of the simulated unit cells for the maximum variations in geometric parameters (a-f) and initial configuration (*) are shown on the right side of the figure.

In order to determine the ability of the FPnP process to create double SRR-like "W" resonators, SL structures similar to those shown in Fig. 4(b) the optical loss properties were modeled with using 3D FEM simulations, using gold coated structures and substrates. Figure 6 shows the effects of varying several write parameters (resist thickness, effective diffraction angle of the branches, and SL thickness) on the thermal loss due to induced current flow in the SRR with the other properties held constant. Plotted are both the position of the resulting resonance and the relative spectral width as a fraction of the resonant frequency of the peak when fit to a Lorentzian. Variation of the resist thickness can be seen to have the largest effect on both parameters. The observed trend in resonant wavelength is as expected due to linear relation between resonant frequency and resonator size that has been demonstrated in the past for SRRs in this size range [28]. In this case, the correlation is non-linear as a result of the branch thickness and gap size remaining constant while the width of the structure increases. This also resulted in sharpening the peak width as the structures became smaller. Variation of the branch angle displayed some effect on the peak width, but, despite changing the width of the structures, did not significantly affect the resonance peak position. This is an effect of the coupled variation of parameters leading to a cancellation in the overall effect of the change on the resonant frequency, which therefore leads to patterning wavelength being a useful tool in adjusting the peak width of the resonance alone. A similar effect can be seen in the variation of the SL thickness, which, despite significantly changing the structural geometry, has little effect on the resonant frequency or peak width. It is

#164825 - $15.00 USD Received 16 Mar 2012; revised 19 Apr 2012; accepted 26 Apr 2012; published 30 Apr 2012

important to note however that the SL is necessary up to the point where the capacitive gap is generated in order to allow for the superwavelength resonance.

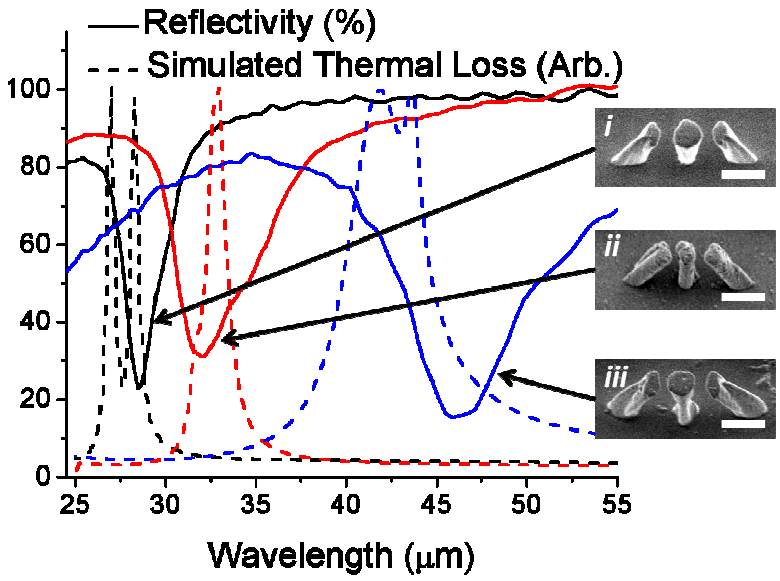

Fig. 7. Measured far-IR reflectivity spectra of the response of resonator arrays fabricated with various sample parameters along with inset SEM images of the structure. Resonant response is indicated by a suppression of the reflectivity. Dashed lines show FEM simulations of simplified structures showing qualitative agreement with the observed results. Parameters of the resonators compared to those in Fig. 6 were *i*) $t = 4.07$, $s = 9.06$, and $\alpha = 25.72$, *ii*) $t = 5.63$, $s = 8.04$, and $\alpha = 25.82$, *iii*) $t = 7.03$, $s = 6.28$, and $\alpha = 25.45$, with additional changes to match the specific features of the structure. (Scale bars 5 μm).

By utilizing different thicknesses of resist and SL and beam parameters, we fabricated a wide variety of "stand-up" W resonator array structures, which were then coated with gold and measured with far IR FTIR microscopy. The reflectivity data of a few examples is shown in Fig. 7. Resonances could be observed as suppression of the reflectivity due to absorptive losses of the driven current of the resonant mode and only occurred when the beam was polarized with the magnetic field perpendicular to the SRRs, this polarization dependence, in combination with the simulations, assured that it was magnetic resonance as opposed to an electronic dipole effect. These results show that by the simple variation of patterning parameters with a single mask element, it is possible to fabricate resonator structures with superwavelength resonances in a range of wavelengths (here 25-45 μm, or 2-4X the largest dimension of the resonator). Further, based on dimensional measurements from SEM images of the structures, it was also possible to refine the FEM model to match the geometry of the actual structures. Specific peak position of the simulations tended to be blue shifted due to approximations in the sample/measurement geometry and electrical properties, and peak width of the experimental results were broadened by the wide range of incident angles of the probe beam which had significant intensity – for the center-blocked Schwarzschild-style IR objective used here, this is a range of angles between 15 to 36° approximately. Despite these limitations, the simulations demonstrate the ability to obtain quantitative agreement with the resonant behavior (even in a complex measurement geometry), allowing for predictive design and determination of the proper write parameters for a desired application.

5. Conclusions

Through a combination of imprint PnP and 3DDW we have demonstrated a novel rapid method, FPnP, for the fabrication of complex 3D structures with single shot exposures. Light

#164825 - $15.00 USD Received 16 Mar 2012; revised 19 Apr 2012; accepted 26 Apr 2012; published 30 Apr 2012

is focused through the imprinted surface mask leading to structures with features controlled by a combination of the diffraction modes of the imprinted pattern and the beam parameters (wavelength, numerical aperture, vertical and later position of the focus etc.) and resist and optional sacrificial layer thicknesses. The number of parameters that can be easily tuned allows for a wide variety of possible single-shot structures for any given mask, each of which would possess local features that could only be otherwise fabricated by lengthy multilayer processes or high resolution 3DDW. Further, these structures can be predicted by FEM modeling allowing for deliberate selection of patterning parameters. By clearing the imprinted mask, consecutive 3DDW is also possible to pattern more arbitrary features. In comparison to 3DDW alone, this technique relaxes the requirement for high numerical aperture (and thereby immersion), can be performed on a wider variety of substrates, and with demonstrated exposures down to 10 ms (not shown), can pattern 1-2 orders of magnitude faster and can potentially be integrated with techniques such as multi-lens arrays for additional gain in patterning rate. To demonstrate the ability for this technique to rapidly produce devices, arrays of "stand-up" resonators were patterned and metallized by sputtering. These SRR-like "W" resonator structures possess polarization dependent resonances from 25 to 45 μm generated from the same mask and optical setup. While this work focused on single-shot structures made from a single 1D imprint mask, we have demonstrated that the technique can be extended to 2D masks. Also, channel structures may be readily generated by moving the write stage during exposure. In addition, by use of sacrificial layers, multiple patterning of several masks on the same sample should be possible. All of these advances represent increases in the technique's capability to become a scalable method for patterning complex 3D architectures.

Acknowledgments

This research was supported (in part) by the U.S. Army Research Office under contract W911NF-07-D-0004. JPS was supported by the Department of Defense (DoD) through the National Defense Science & Engineering Graduate Fellowship (NDSEG) Program. Use of the National Synchrotron Light Source, Brookhaven National Laboratory, was supported by the U.S. Department of Energy, Office of Science, Office of Basic Energy Sciences, under Contract No. DE-AC02-98CH10886. The authors would like to thank Dr. G. Larry Carr, Randy Smith, and Quing-Yi Dong at NSLS U12A for their assistance.

#164825 - $15.00 USD Received 16 Mar 2012; revised 19 Apr 2012; accepted 26 Apr 2012; published 30 Apr 2012